Accepted Manuscript

Impact of small-scale obscuration, surface roughness and reflectivity fluctuations of optical elements on the temporal contrast of a femtosecond pulse

Efim Khazanov

Gaponov-Grekhov Institute of Applied Physics of the Russian Academy of Sciences (IAP RAS), Nizhny Novgorod

efimkhazanov@gmail.com

Abstract. The impact of compressor gratings and transport optics imperfections on the power contrast ratio (PCR) is considered analytically taking into account diffraction and all dispersion orders. All types of imperfections, including surface roughness, reflectivity fluctuations, surface dirt/damage/obscuration as well as the roughness and obscuration on the optics used to write holographic gratings are allowed for. For the same roughness and obscuration, the contribution to the PCR of the latter is significantly greater than the contribution of the gratings. Comparison of the PCR caused by obscuration and by roughness showed that at short times the latter prevails, whereas at long times the obscuration is dominant. The radiation scattered by the second and third gratings arrives at the target before the main pulse in the form of a vertical strip near the beam axis. Then this strip moves uniformly towards the axis, reaching it simultaneously with the main pulse.

Keywords: holographic difraction gratings, surface roughness, power spectral density

1. Introduction

The key technologies of all high-power lasers are CPA or OPCPA. Pulse stretching, amplification and compression inevitably lead to temporal contrast degradation, i.e., to the formation of a pre-pulse long before the main pulse and the post-pulse after the main pulse. Contrast degradation occurs in a wide time interval from 100 fs to nanoseconds. The pre-pulse is hazardous, as the target may be destroyed before the arrival of the main pulse, which restrains laser application, especially in experiments with solid targets. Many causes of contrast degradation are of a temporal nature, so they may be analysed, as a rule, in the time domain. These include the amplified spontaneous emission from a seed laser and amplifiers (both laser and parametric), amplitude and phase distortions of the temporal spectrum of the pulse, and residual reflections and nonlinearity of the refractive index [1]. A special place belongs to light scattering on optical elements, which leads to the appearance of a noise field with a wide spatial spectrum. The propagation of such a field in a compressor or a stretcher leads to space-time coupling (see [2, 3] and references therein).

The physical reason for contrast degradation due to space-time coupling is the overtaking/lagging of the scattered pulse behind the main pulse. Lagging is the most frequent case. However, if one pair of gratings is located between the scatterer and the target (“half” of compressor or stretcher), part of the scattered radiation overtakes the main pulse, resulting in the appearance of a pre-pulse. Since the time of overtaking is proportional to the spatial frequency, only small-scale fluctuations in the field amplitude or phase are significant for the contrast.

There are several reasons for scattering. First of all, it is an imperfect surface quality of the optical elements. The influence of imperfection on contrast was first numerically revealed in [4]. Most subsequent works were devoted to numerical [5-13] and experimental [5, 8, 10-12, 14-19]

10.1017/hpl.2025.10073

studies of this effect both in the stretcher [5-8, 10-19] and in the compressor [6, 8-13]. A theory without allowance for the diffraction and dispersion of a spatial chirp was proposed in [20], developed in [21], and later supplemented in [19]. It was shown that the contrast is determined by the power spectral density (PSD) of the surface profile of the second and third gratings of stretcher/compressor and stretcher mirrors. These works are mainly focused on the intensity contrast in the far field, which is extremely difficult to measure. As a rule, the power contrast ratio (PCR) $\mathbb{C}(t)$ is measured:

$$\mathbb{C}(t) \equiv \frac{<P_{out}(t)> - P_{0,out}(t)}{P_{0,out}(0)}, \quad (1)$$

where $< P_{out}(t) >$ is the pulse power, and $P_{0,out}(t)$ is the power of the main pulse (neglecting scattered field). Since the near and far fields are related by the spatial Fourier transform, then, according to Parseval's theorem, $P(t)$ is the same in the near and far fields; consequently, $\mathbb{C}(t)$ is also the same. Moreover, the analysis of the expression (13) from [21] shows that in the near field the intensity contrast differs little from the power contrast. This means that the magnitude of $\mathbb{C}(t)$ is measured, even if the contrast meter covers only part of the aperture. Expressions for the PCR as a function of the PSD of the compressor/stretcher grating surface and the transport optics were obtained in [22] taking into account diffraction and all orders of dispersion.

At the same time, in addition to surface roughness, other optics imperfections whose influence has not been studied before also contribute to the PCR. First of all, it is the radiation scattering on dirt/damage/obscurations which inevitably appear both during the production of gratings and mirrors and in the course of their operation in high-power laser facilities [23]. Following [23], we will assume that the obscurations ‘‘absorb’’ all incident laser light. Besides the roughness and obscurations of the beamline optics (gratings and mirrors), the roughness and obscurations of the mirrors used for writing holographic gratings also lead to degradation. They give rise to groove shape fluctuations leading to reflectivity fluctuations [24] as well as to non-equidistance and non-parallelism of the grooves, which in turn result in wave front fluctuations of diffracted radiation [25-28]. In this work, we investigate in a general form the PCR caused by four reasons: roughness and obscurations of both beamline optics and writing optics. The only constraint that will be used is the spatial scale of obscurations and roughnesses and, hence, of the scattered radiation fluctuations much smaller than the beam diameter.

A general expression relating the PCR to the PSD of scattered field fluctuations is obtained in Section 2 without specifying the cause of scattering. Then, the PSD fields are found for obscurations of beamline optics (Section 3), for roughness of beamline optics (Section 4), and for obscurations and roughness of writing optics (Section 5). Section 6 provides an example of calculating the PCR using the obtained formulas and a discussion of the results.

2. General expression for power contrast ratio $\mathbb{C}(t)$

Most lasers use the Treacy compressor [29] shown in Fig. 1, which has three parameters: N is the groove density, L is the distance between the gratings along the normal, and α is the angle of incidence on the first grating. In a general case of an out-of-plane compressor [30], there is one more parameter γ that is the angle of incidence on the first grating in the plane orthogonal to the diffraction plane. The angle of reflection β for the central frequency $\omega_0 = ck_0 = 2\pi c/\lambda_0$ is determined from the expression for the grating $sin\beta = -\lambda_0 N/cos\gamma + sin\,\alpha$. An important special case of an out-of-plane compressor is the Littrow compressor [31, 32], in which $\alpha = \alpha_L$, where α_L is the Littrow angle. It is convenient to start the consideration with the field $E_0(\Omega, \boldsymbol{r})$ ($\Omega = \omega - \omega_0$) incident on an imperfect optical element that may be any diffraction grating G1-G4, input and output optics M_{in} and M_{out}, as well as gratings and stretcher mirrors. We will search for the contrast $\mathbb{C}(t)$ caused by each element separately, assuming that all other elements are perfect. After reflection, the field takes the form

$$E_1(\Omega, \boldsymbol{r}) = E_0(\Omega, \boldsymbol{r}) + E_0(\Omega, \boldsymbol{r})\big(\Theta(\boldsymbol{r}) + \mathcal{A}(\boldsymbol{r}) + i\varphi(\boldsymbol{r})\big), \quad (2)$$

https://doi.org/10.1017/hpl.2025.10073 Published online by Cambridge University Press

where $\mathcal{A}(\boldsymbol{r}) \ll 1$, $\varphi(\boldsymbol{r}) \ll 1$, and $\Theta(\boldsymbol{r})$ are real, homogeneous, ergodic random functions (fields) characterizing the fluctuations of the field amplitude and phase, as well as the presence of obscurations: $\Theta(\boldsymbol{r}) = 1$ inside and $\Theta(\boldsymbol{r}) = 0$ outside the obscurations. Following [23], we assume that the obscurations "absorb" all incident laser light, thus they affect only the amplitude of the incident beam, but not its phase. The size and coordinates of the obscurations on the surface of the optical element are random variables. The second term in Eq. (2) will be further called noise for brevity, and the noise energy will be taken to be much lower than the energy of the main pulse $W_0 = \int |E_0(\Omega, \boldsymbol{r})|^2 \, \boldsymbol{dr} d\Omega$:

$$W_{\mathrm{X}} = \int |\mathrm{X}(\boldsymbol{r}) E_0(\Omega, \boldsymbol{r})|^2 \, \boldsymbol{dr} d\Omega = \sigma_{\mathrm{X}}^2 W_0 \ll W_0 \qquad (X = \Theta, \mathcal{A}, \varphi) \tag{3}$$

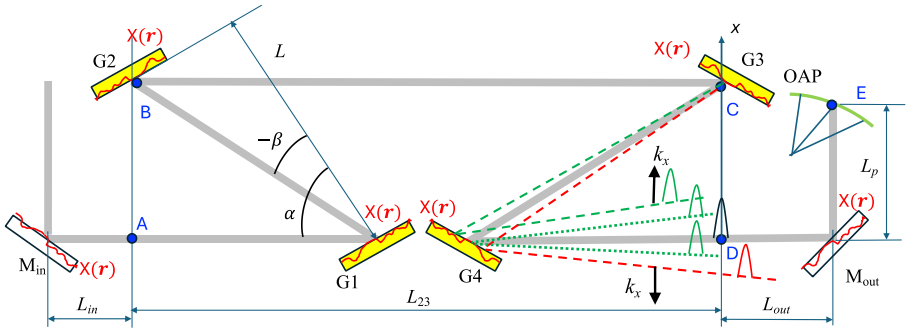

Fig. 1. Compressor scheme. G1-G4 – diffraction gratings, OAP – off-axis parabola, M_{in} – input optics, M_{out} – output optics. Dotted lines – radiation scattered by G4, scattered pulses lag behind the main one. Dashed lines – radiation scattered by G3, scattered pulses lag behind (green) or overtake (red) the main pulse, depending on the sign of k_x.

Since in this paper we are interested in small-scale intensity fluctuations, the characteristic spatial scale of $E_0(\boldsymbol{r})$ is much larger than the characteristic spatial scale of $\Theta(\boldsymbol{r})$, $\mathcal{A}(\boldsymbol{r})$ and $\varphi(\boldsymbol{r})$, i.e., the correlation length of these functions is much smaller than the beam size. In other words, the spatial spectrum of the noise is much wider than the spectrum of the main beam. From ergodicity it follows that

$$\sigma_{\mathrm{X}}^2 = < X^2(\boldsymbol{r}) > \tag{4}$$

with $\sigma_\Theta^2 = S_{ob}/S_0$, where S_{ob} is the total area of all obscurations, and S_0 is the beam area. The angle brackets denote ensemble averaging. For clarity, $\Theta(\boldsymbol{r})$, $\mathcal{A}(\boldsymbol{r})$ and $\varphi(\boldsymbol{r})$ are shown in Fig. 2. Eq. (2) has a most general form and includes all possible imperfections of the optical element. Note that beam clipping, which also affects the contrast [33], is not described by Eq. (2) and is outside the scope of this paper. The functions and their Fourier transforms will be designated by the same letters, but with different arguments:

$$E_j(\Omega, \boldsymbol{\kappa}) = \tfrac{1}{2\pi} \int E_j(\Omega, \boldsymbol{r}) e^{i\boldsymbol{\kappa r}} \mathrm{d}\boldsymbol{r} \quad E_j(\Omega, \boldsymbol{r}) = \tfrac{1}{2\pi} \int E_j(\Omega, \boldsymbol{\kappa}) e^{-i\boldsymbol{\kappa r}} \mathrm{d}\boldsymbol{\kappa} \tag{5}$$

and analogously for the temporal Fourier transform. Hereinafter, the range of integration, if not otherwise specified, is $\pm\infty$. From Eqs. (2, 5) we obtain

$$E_1(\Omega, \boldsymbol{k}_\perp) = E_0(\Omega, \boldsymbol{k}_\perp) - \tfrac{1}{2\pi} \int \boldsymbol{dr} e^{i\boldsymbol{k}_\perp r} E_0(\Omega, \boldsymbol{r}) \mathcal{A}(\boldsymbol{r}) \tag{6}$$

https://doi.org/10.1017/hpl.2025.10073 Published online by Cambridge University Press

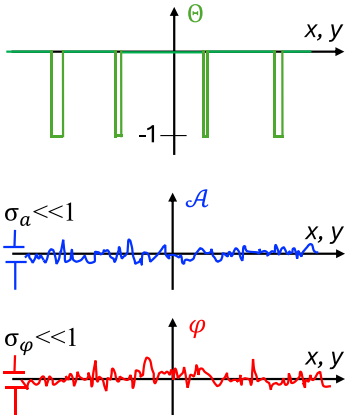

Fig. 2. Schematic representation of random functions $\Theta(\boldsymbol{r})$, $\mathcal{A}(\boldsymbol{r})$ and $\varphi(\boldsymbol{r})$.

The field on the focusing parabola (point E) up to which the field $E_1(\Omega, \boldsymbol{k}_\perp)$ Eq. (6) passes through an optical system containing a pair(s) of parallel gratings and a section(s) of free space of total length L_f is considered to be the output field $E_{out}(\Omega, \boldsymbol{k}_\perp)$. Regardless of the order in which these elements are passed, the field $E_{out}(\Omega, \boldsymbol{k}_\perp)$ has the form

$$E_{out}(\Omega, \boldsymbol{k}_\perp) = E_1(\Omega, \boldsymbol{k}_\perp) e^{i\Psi(\Omega, \boldsymbol{k}_\perp)}, \tag{7}$$

where $\Psi(\Omega, \boldsymbol{k}_\perp)$ is the sum of the phase $\Psi_f = L_f\sqrt{k_0^2 - k_\perp^2}$ introduced by the free space of length L_f and *i)* by two pairs of parallel diffraction gratings from point A to point B and from point C to point D for M_{in} or G1; or *ii)* by one pair from point C to point D for G2 or G3); or *iii)* there are no other terms for G4 or M_{out}. It is convenient to present the function $\Psi(\Omega, \boldsymbol{k}_\perp)$ as a Taylor series at the point $\Omega = 0$, $k_x = k_y = 0$ ($k_{x,y}$ are the components of the vector $\boldsymbol{k}_\perp$) by extracting the term of the first power in Ω and designating all the other terms as $\Phi(\Omega, \boldsymbol{k}_\perp)$:

$$\Psi(\Omega, \boldsymbol{k}_\perp) = \Omega\tau(\boldsymbol{k}_\perp) + \Phi(\Omega, \boldsymbol{k}_\perp) \tag{8}$$

The expressions for the phase introduced by the pair of parallel diffraction gratings $\Psi_p(\Omega, \boldsymbol{k}_\perp)$, as well as for ψ_a^b derivatives of Ψ_p with respect to ω, k_x, k_y at the point $\Omega = 0$, $k_x = k_y = 0$ also needed for the Taylor series, can be found in [34, 35]. Using them one can obtain the expression for $\tau(\boldsymbol{k}_\perp)$ in the form:

$$\tau(\boldsymbol{k}_\perp) = 2\tau_x\frac{k_x}{k_0} + 2\tau_y\frac{k_y}{k_0} + t_x\frac{k_x^2}{k_0^2} + t_y\frac{k_y^2}{k_0^2} + 2t_{xy}\frac{k_xk_y}{k_0^2} \tag{9}$$

$$\tau_x = \frac{1}{2}k_0\psi''_{x\omega} = \mp\frac{AL}{2c} \qquad \tau_y = \frac{1}{2}k_0\psi''_{y\omega} = \mp\frac{GL}{2c} \tag{10}$$

$$t_x = \frac{1}{2}k_0^2\psi'''_{xx\omega} = \frac{EL+L_f}{2c} \qquad t_y = \frac{1}{2}k_0^2\psi'''_{yy\omega} = \frac{FL+L_f}{2c} \qquad t_{xy} = \frac{1}{2}k_0^2\psi'''_{xy\omega} = \pm\frac{KL}{2c} \tag{11}$$

$$A = \frac{cos\alpha}{cos^3\beta}(sin\alpha - sin\beta) \qquad F = \frac{1+\cos(\alpha+\beta)}{cos\beta} + \frac{(sin\beta - sin\alpha)^2}{cos^3\beta} \tag{12}$$

$$E = \frac{cos^2\alpha}{cos^3\beta} + \frac{\cos(\alpha+\beta)}{cos\beta} + \frac{sin\alpha - sin\beta}{cos^3\beta}\left(sin\alpha - 3sin\beta\frac{cos^2\alpha}{cos^2\beta}\right) \tag{13}$$

$$G = \gamma\frac{(sin\beta - sin\alpha)^2}{cos^3\beta} \qquad K = 2A\gamma\left(1 - \frac{3}{2}sin\beta\frac{sin\alpha - sin\beta}{cos^3\beta}\right) \tag{14}$$

As $\gamma \ll 1$ in a general case, terms of order γ^2 are omitted here. From here on we will restrict ourselves to the paraxial approximation, i.e., we will consider $k_{x,y}$ of powers not higher than 2. Thus, we take into account diffraction in the paraxial approximation and all orders of dispersion, including the dispersion of the spatial chirp, since the term $\Phi(\Omega, \boldsymbol{k}_\perp)$ includes terms with Ω^2, Ω^3, etc. Further we assume that the grating pairs in the compressor are identical. This is not the case for an asymmetric compressor [34, 36-42], but we restrict consideration to a symmetric one. The

https://doi.org/10.1017/hpl.2025.10073 Published online by Cambridge University Press

sign $\mp$ in Eqs. (10, 11) corresponds to the first and second pairs of gratings; therefore, for two pairs of gratings, the total values of t_{xx}, t_{yy} are doubled, and $\tau_x = \tau_y = t_{xy} = 0$. Note that, if α is equal to the Littrow angle, then $F = E$. This is not the case for the Treacy compressor, but usually α is chosen as close to the Littrow angle as the decoupling condition allows (the beam incident on grating G1 should not overlap with the second grating). Hence, for the compressor, the values of F and E are close, for example, in the XCELS project [43] $F = 1.025E$ and we can assume that $\tau_y \approx \tau_x$. This condition is fulfilled exactly for the Littrow compressor [31, 32].

The quantity $\tau(\boldsymbol{k}_\perp)$ has a simple physical meaning – it is the time delay of the noise component with wave vector $\boldsymbol{k}_\perp$ relative to the wave with $\boldsymbol{k}_\perp = 0$. Since $E > 0$ and $EF > K^2$, the last three terms in (9) are a positively defined quadratic form, i.e., the only negative terms in Eq. (9) are the terms with τ_x and τ_y. If $\tau_x = \tau_y = 0$, then all noise components lag behind the main wave, which means that at $t < 0$ the contrast is zero (a perfect case). This is true for all optical elements in Fig. 1, except for gratings G2 and G3.

The power $P_{out}(t)$ required for calculating $\mathbb{C}(t)$ by the definition Eq. (1) is

$$P_{out}(t) = \int |E_{out}(t, \boldsymbol{k}_\perp)|^2 d\boldsymbol{k}_\perp. \tag{15}$$

By substituting Eq. (8) into Eq. (7) and performing the inverse time Fourier transform we obtain $E_{out}(t, \boldsymbol{k}_\perp)$. By substituting it into Eq. (15) and the result into Eq. (1) we find $\mathbb{C}(t)$. The transformations absolutely analogous to [22] yield

$$\mathbb{C}(t) = \frac{t_p}{W_0 2\pi} \int d\boldsymbol{k}_\perp \, PSD2(\boldsymbol{k}_\perp) \int\int d\Omega d\Omega' e^{i\Phi(\Omega,k_x,k_y) - i\Phi(\Omega',k_x,k_y)} e^{i(\Omega'-\Omega)(t-\tau)} \int E_0(\Omega, \boldsymbol{r}) E_0^*(\Omega', \boldsymbol{r}) \, \boldsymbol{dr}, \tag{16}$$

where $t_p = W_0 / P_{0,out}(0)$ is the duration of the output pulse and

$$PSD2(\boldsymbol{k}_\perp) = PSD2_\Theta(\boldsymbol{k}_\perp) + PSD2_a(\boldsymbol{k}_\perp) + PSD2_\varphi(\boldsymbol{k}_\perp), \tag{17}$$

where $PSD2_X(\boldsymbol{k}_\perp)$ is the two-dimensional power spectral density of the function X ($X = \Theta, \mathcal{A}, \varphi$) defined by

$$PSD2_X(\boldsymbol{k}_\perp) = (2\pi)^2 \int ACF_X(\boldsymbol{\rho}) e^{i\boldsymbol{k}_\perp \boldsymbol{\rho}} \boldsymbol{d\rho} \quad , \tag{18}$$

where $ACF_X(\boldsymbol{\rho}) = < X(\boldsymbol{r} - \boldsymbol{\rho}) X(\boldsymbol{r}) >$. Here we took into account that $\Theta(\boldsymbol{r})$, $\mathcal{A}(\boldsymbol{r})$, and $\varphi(\boldsymbol{r})$ are uncorrelated with each other. Note that the noise energy is, evidently, $W_n = P_{0,out}(0) \int \mathbb{C}(t) dt = W_\Theta + W_a + W_\varphi$. The integration of Eq. (16) with respect to t gives $2\pi\delta(\Omega' - \Omega)$, where δ is the Dirac delta function. Next, taking into account Eq. (3) we obtain an obvious relation

$$\sigma_X^2 = \int PSD2_X(\boldsymbol{k}_\perp) \boldsymbol{dk}_\perp. \tag{19}$$

The $PSD2$ definition Eq. (18) is known in the literature, but it is not the only one. It differs from the definition used, for example, in [21, 22, 44], where there is no $(2\pi)^2$ multiplier. We chose the Eq. (18), since in this case Eq. (19) for σ_X^2 has a simpler form. In the special case of purely phase distortions ($\mathcal{A} = \Theta = 0$), Eq. (16) coincides with formula (14) from [22].

By substituting Eq. (11) into Eq. (16) we change the variables

$$\boldsymbol{u} = \begin{pmatrix} 1 & t_{xy}/t_x \\ 0 & \sqrt{T_y/t_x} \end{pmatrix} |\sqrt{|t_x|}| \frac{\boldsymbol{k}_\perp}{k_0} + sign(t_x) \begin{pmatrix} \tau_x / \sqrt{|t_x|} \\ \left(\tau_y - \frac{t_{xy}}{t_x}\tau_x\right) / \sqrt{|T_y|} \end{pmatrix}. \tag{20}$$

Further, supposing that $PSD2$ is an isotropic function, i.e., $PSD2(k_x, k_y) = PSD2(k_\perp)$ and passing from (u_x, u_y) to the polar coordinates (u, θ) we obtain

https://doi.org/10.1017/hpl.2025.10073 Published online by Cambridge University Press

$$\mathbb{C}(t) = \frac{k_0^2}{2}\frac{t_p}{\sqrt{|t_x T_y|}}\int_0^{2\pi} PSD2\left(k_0\sqrt{g(\theta)}\right)d\theta \text{ if } \frac{t}{t_c} > -1; \text{ otherwise } \mathbb{C} = 0, \quad (21)$$

where

$$t_c = \frac{1}{T_y t_x}\left(t_y\tau_x^2 + t_x\tau_y^2 - 2t_{xy}\tau_y\tau_x\right) \quad (22)$$

$$g(\theta) = \kappa_\tau^2 cos^2\theta\frac{|t_c|}{|t_x|} + \kappa_\tau^2 sin^2\theta\frac{|t_c|}{|t_x|}\left(\left(\frac{t_{xy}}{t_x}\right)^2 + \frac{|t_x|}{|T_y|}\right) - 2q_x\kappa_\tau cos\theta\frac{\sqrt{|t_c|}}{\sqrt{|t_x|}} + q_x^2 + q_y^2 -$$
$$\kappa_\tau^2\frac{|t_c|}{\sqrt{|t_x|}}\frac{t_{xy}}{t_x}sin2\theta\frac{1}{\sqrt{|T_y|}} - 2\kappa_\tau sin\theta\frac{\sqrt{|t_c|}}{\sqrt{|T_y|}}\frac{1}{T_y t_x^2}\left(\tau_y\left(t_x^2 + t_{xy}^2\right) - t_{xy}\tau_x\left(t_x + t_y\right)\right) \quad (23)$$

$$T_y = \frac{t_x t_y - t_{xy}^2}{t_x} \qquad q_x = \frac{t_y\tau_x - t_{xy}\tau_y}{T_y t_x} \qquad q_y = \frac{t_x\tau_y - t_{xy}\tau_x}{T_y t_x} \qquad \kappa_\tau = \sqrt{1 + \frac{t}{t_c}} \quad (24)$$

Here we restrict consideration to the case $t_x t_y > 0$ (the diffraction has the same sign along *x* and *y*), which is always fulfilled for the compressor, but not always for the stretcher [22], and take into account that $t_x t_y - t_{xy}^2 > 0$ (i.e., T_y has the same sign as t_x). Note that only κ_τ is time dependent.

Next, we take into account that $\gamma \ll 1$ and, consequently, $\frac{t_{xy}}{t_x} \sim \gamma \ll 1$ and $\frac{\tau_y}{t_x} \sim \gamma \ll 1$. By expanding $\mathbb{C}(t, \gamma)$ in a Taylor series near the point $\gamma = 0$ it is easy to show that the term proportional to γ vanishes. Consequently, the difference in the contrast $\mathbb{C}(t, \gamma)$ for an out-of-plane compressor from the contrast $\mathbb{C}(t, \gamma = 0)$ for a plane compressor reduces to corrections of the order of γ^2. For typical values of $\gamma = 10 \ldots 15$ degrees, the correction will be about 5%, which is negligibly small for contrast. Thus, the PCR $\mathbb{C}(t)$ does not depend on γ and we can use the expressions for a plane compressor. In other words, the contrast of an out-of-plane compressor practically does not differ from the contrast of a plane one. At $\gamma = 0$, Eq. (21) strictly passes into (19) from [22] (taking into consideration that the definition of $PSD2$ in [22] differs from Eq. (18) by the multiplier $(2\pi)^2$). Therefore, the results obtained in [22] for phase noise are valid in a general case if $PSD2_\varphi(\boldsymbol{k}_\perp)$ is replaced by $PSD2(\boldsymbol{k}_\perp)$ Eq. (17). In particular, if we take into account that $t_x \approx t_y = t_d$, then Eq. (21) takes the form

$$\mathbb{C}(t) = \frac{k_0^2}{2}\frac{t_p}{|t_d|}\int_0^{2\pi} PSD2\left(k_0\left|\frac{\tau_x}{t_d}\right|\sqrt{\kappa_\tau^2 + 1 - 2\kappa_\tau cos\theta}\right)d\theta, \text{ if } \frac{t}{t_c} > -1; \text{ otherwise } \mathbb{C} = 0. \quad (25)$$

This expression is significantly simplified in two important particular cases. First, for G2 and G3 gratings, the allowance for diffraction ($t_d \neq 0$) leads to the emergence of the cut-off time t_c and to a slight contrast asymmetry which can be neglected, then

$$\mathbb{C}_s(t) = \frac{k_0}{2}\frac{t_p}{\tau_x}PSD1\left(\frac{tk_0}{2\tau_x}\right) \qquad \text{if } \frac{t}{t_c} > -1; \text{ otherwise } \mathbb{C}_s = 0 \quad , \quad (26)$$

where $PSD1(k_x)$ is a one-dimensional PSD function related to $PSD2(k_\perp)$ as [45]:

$$PSD1(k_x) = 2\int_{k_x}^{\infty}\frac{PSD2(k_\perp)}{\sqrt{k_\perp^2 - k_x^2}}k_\perp dk_\perp \qquad PSD2(k_\perp) = \frac{-1}{\pi}\int_\kappa^\infty \frac{1}{\sqrt{k_x^2 - k_\perp^2}}\frac{dPSD1(k_x)}{dk_x}dk_x \quad (27)$$

with

$$\sigma^2 = \int PSD1(k_x)dk_x. \quad (28)$$

Second, there is no space chirp $\tau_x = \tau_y = 0$ for all optical elements in Fig. 1, except for gratings G2 and G3; for them the contrast $\mathbb{C}_d(t)$ is determined only by the diffraction:

$$\mathbb{C}_d(t) = \pi k_0^2\frac{t_p}{|t_d|}PSD2\left(k_0\sqrt{\frac{t}{t_d}}\right) \text{ if } \frac{t}{t_d} > 0; \text{ otherwise } \mathbb{C}_d = 0 \quad (29)$$

https://doi.org/10.1017/hpl.2025.10073 Published online by Cambridge University Press

If $t_d > 0$, then $\mathbb{C}_d(t < 0) = 0$, which explains the frequently observed [5, 15-18, 46, 47] experimental asymmetry of the contrast: at $t < 0$ (pre-pulse) it is always weaker (better) than at $t > 0$ (post-pulse), since all optical elements contribute to the contrast at $t > 0$, while only gratings G2 and G3 contribute to it at both $t < 0$ and $t > 0$. In [47] the authors experimentally proved that the contrast asymmetry cannot be explained by ASE, Raman effect, Kerr-lens mode-locking, and Kerr nonlinearity in Ti:sapphire amplifiers. The hypothesis [47], that phonons play a key role as Ti:sapphire lasers are vibronic, contradicts the recent experiments [5, 46] with a fully OPCPA laser where the contrast asymmetry was measured. The measured post-pulse in [47] did not depend on the stretching factor or on the dispersive elements (gratings or prisms), and the author concluded that scattering on the diffraction gratings also has no impact on asymmetry of the contrast. As seen from (26, 29), it is true only for the scattering on the second and third gratings, but not for the scattering on all other optics, including optics in the contrast measurement beamline. Thus, this scattering is the only way to explain the contrast asymmetry. Note that it cannot be explained by the earlier developed [19-21] diffraction-free approximation, in which $\mathbb{C}(t)$ is an even function.

In the case of negative diffraction ($t_d < 0$), the time t changes its sign to the opposite one and the contrast $\mathbb{C}_d(t)$ is nonzero at negative times. This is possible if the scheme comprises a telescope transferring the image of the optical element beyond the focusing parabola. In addition, the contrast meter is usually located not directly in the powerful beam, but in its weakened replica. The meter also receives the radiation scattered throughout the optics located in the measuring path. Its contribution to the PCR is also described by Eq. (29), where $t_d = L_m/2c$ and L_m is the distance from the optical element in the path to the meter. If $L_m > 0$, then the measured contrast will be higher than the real one at $t > 0$. However, if there is an image transfer in the path, then L_m may be less than zero, and the contrast measured will be higher than the real one at < 0, see Eq. (29).

Eqs. (26, 29) clearly show the $PSD1(k_x)$ mapping on $\mathbb{C}_s(t)$ and $PSD2(k_\perp)$ on $\mathbb{C}_d(t)$, with $k_x = \frac{tk_0}{2\tau_x}$ in the first case and $k_\perp = k_0\sqrt{\left|\frac{t}{t_d}\right|}$ in the second case. Correspondingly, the condition of paraxial approximation $k_{x,\perp} \ll k_0$ constrains the obtained results to the conditions $|t| \ll 2|\tau_x|$ for $\mathbb{C}_s(t)$ and $\sqrt{|t|} \ll \sqrt{|t_d|}$ for $\mathbb{C}_d(t)$. Further investigation of $\mathbb{C}(t)$, including quantitative comparison with $\mathbb{C}_d(t)$ and $\mathbb{C}_s(t)$, is possible only for the functional forms $PSD2_\Theta$, $PSD2_a$, and $PSD2_\varphi$.

3. PSD functional form PSD_Θ for obscurations on the grating/mirror surface

To find $PSD2_\Theta(k_\perp)$ for the field reflected from a surface with obscuration, we assume that the obscurations do not overlap each other and are shaped as a circle with coordinates of the center $\boldsymbol{R}_m$ and radius w_m:

$$\Theta(\boldsymbol{r}) = \sum_{m=1}^{M} \Pi\left(\frac{\boldsymbol{r}-\boldsymbol{R_m}}{w_m}\right), \tag{30}$$

where $\Pi(x) = 1\ if\ |x| < 1$, otherwise $\Pi = 0$ and $M \gg 1$ is the number of obscurations. $\boldsymbol{R}_m$ and w_m are random quantities, with $\boldsymbol{R}_m$ being uniformly distributed over the beam aperture and w_m having a probability density $f(w)$. It is obvious that $S_{ob} = \pi\sum_{m=1}^{M} R_m^2$. The squared modulus of the noise spectrum S_Θ is an incoherent sum of the squared moduli of the spectra S_m of flat-top beams having radius w_m (Airy functions):

$$S_\Theta(k_\perp) = \sum_{m=1}^{M} S_m = I_0 \sum_{m=1}^{M} w_m^4 \frac{J_1^2(k_\perp w_m)}{(k_\perp w_m)^2}, \tag{31}$$

where J_1 is the Bessel function and $I_0 = |E_0|^2$ is the incident beam intensity assumed for simplicity to be equal for all obscurations. Here we sum the spectra incoherently, since the spectral phase of each obscuration is random and the sum of a large number of terms with random phase is zero. As a consequence, S_Θ does not depend on $\boldsymbol{R_m}$. From the definition of the *PSD2* in Eq. (18) and of the

https://doi.org/10.1017/hpl.2025.10073 Published online by Cambridge University Press

Fourier spectrum in Eq. (5), with allowance for ergodicity we obtain $PSD2_\Theta(k_\perp) = \frac{<S_\Theta(k_\perp)>}{I_0 S_0}$. By averaging Eq. (31) we find

$$PSD2_\Theta(k_\perp) = \frac{\sigma_\Theta^2}{\pi k_\perp^2} \frac{\int_{w_{min}}^{w_{max}} w^2 J_1^2(k_\perp w) f(w) dw}{\int_{w_{min}}^{w_{max}} w^2 f(w) dw}, \quad (32)$$

from which, with Eq. (27) taken into account, follows

$$PSD1_\Theta(k_x) = \frac{\sigma_\Theta^2}{\pi k_x^2} \frac{\int_{w_{min}}^{w_{max}} w f(w) \mathbf{H_1}(2wk_x) dw}{\int_{w_{min}}^{w_{max}} w^2 f(w) dw}, \quad (33)$$

where $\mathbf{H_1}$ is the Struve function and $w_{min,max}$ are the minimum and maximum radii of the obscurations. Obviously, $2w_{min} \gg \lambda_0$, since the paraxial approximation does not hold otherwise. Similarly, the obscurations with radius w commensurate with the beam radius R_0 cannot exist, since in this case the condition $W_\Theta \ll W_0$ is violated. This imposes the constraint $w_{max} \ll R_0$. In practice, the quantities $w_{min,max}$ may have even more stringent constraints. Note that Eqs. (32) and (33) satisfy Eqs. (19) and (28) regardless of the form of the function $f(w)$.

Next, it is necessary to substitute into Eqs. (32, 33) $f(w)$ of specific form which may be quite complex. For example, for the optics of the standard indicated in [48], $f(w)$ has the form $logf(w) \sim (logw)^2$. We will restrict our consideration to the power form

$$f(w) = A_1 \frac{1}{w^\xi}, \quad (34)$$

given in [23] for surface defects of optical elements after their use in a high-power laser facility. Under the almost always met condition $w_{max}^{\xi-1} \gg w_{min}^{\xi-1}$, from $\int_{w_{min}}^{w_{max}} f(w) dw = 1$ we obtain $A_1 = (\xi - 1) w_{min}^{\xi-1}$, i.e., $f(w)$ does not depend on w_{max}. The data reported in [23] correspond to $\xi = 3.9$ and $w_{min} \approx 0.025$ mm. Before using the optical elements in the high-power laser facility, the distribution function $f(w)$ is also defined by Eq. (34) with $\xi = 3.9$, but the laser damage was 7.8 times less [23, 49]. In what follows, we will assume ξ and w_{min} to be arbitrary constants and use the above values only for constructing specific plots in Section 6. The moments $< w^n >$ are readily calculated from Eq. (34):

$$< w^n > = \int_{w_{min}}^{w_{max}} w^n f(w) dw = w_{min}^n \frac{\xi - 1}{\xi - n - 1} \left(1 - Z^{n-\xi+1}\right), \quad (35)$$

where $Z = w_{max}/w_{min}$. For $\xi = n + 1$, the Eq. (35) is valid within the limit $\xi \to n + 1$. On substituting Eq. (34) into Eqs. (32, 33) an passing to dimensionless quantities $\kappa = k_\perp w_{min}$ and $K = k_x w_{min}$, we obtain

$$\frac{\pi <w^2>}{\sigma_\Theta^2 w_{min}^4} PSD2_\Theta(\kappa) = \frac{\xi - 1}{\kappa^{5-\xi}} \int_\kappa^{Z\kappa} \frac{J_1^2(u)}{u^{\xi-2}} du \qquad \frac{\pi <w^2>}{\sigma_\Theta^2 w_{min}^3} PSD1_\Theta(K) = \frac{\xi - 1}{K^{4-\xi}} \int_K^{KZ} \frac{\mathbf{H_1}(2u)}{u^{\xi-1}} du. \quad (36)$$

Both integrals in Eq. (36) are expressed only through the generalized hypergeometric function ${}_2F_3$, which complicates further analytical analysis. The expression Eq. (36) can be significantly simplified in three special cases: for $k_\perp w_{max} \ll 1$ and $k_\perp w_{min} \gg 1$, the functions J_1 and $\mathbf{H_1}$ may be replaced by their asymptotic forms, and for $w_{max}^{-1} \ll k_{\perp,x} \ll w_{min}^{-1}$, the integration limits may be replaced by 0 and ∞. In all special cases, a power-law dependence is obtained: in three sections of the spectrum $k_{\perp,x} w_{max} \ll 1$, $w_{max}^{-1} \ll k_{\perp,x} \ll w_{min}^{-1}$ and $k_{\perp,x} w_{min} \gg 1$, $PSD2_\Theta$ decreases in a power-law manner with powers $0, (5 - \xi)$ and 3, and $PSD1_\Theta$ with powers $0, (4 - \xi)$ and 2. This is demonstrated in Fig. 3 where $PSD2_\Theta(k_\perp)$ Eq. (36) is plotted. The $PSD1(k_x)$ curves look similar. From Fig. 3 it can be seen that $PSD2_\Theta(k_\perp)$ is well approximated by the expression

$$\frac{\pi <w^2>}{\sigma_\Theta^2 w_{min}^4} PSD2_\Theta(\kappa) \approx \frac{1}{4} \frac{\xi - 1}{\xi - 5} \frac{1 - Z^{5-\xi}}{\left(1 + \kappa^2/\kappa_L^2\right)^{\frac{5-\xi}{2}}} e^{-\kappa^2} + \frac{1}{\pi} \frac{\xi - 1}{\xi - 2} \frac{1 - Z^{2-\xi}}{\kappa^3} \left(1 - e^{-\kappa^4}\right), \quad (37)$$

https://doi.org/10.1017/hpl.2025.10073 Published online by Cambridge University Press

where

$$\kappa_L = 2\left(\frac{1}{1-Z^{5-\xi}}\frac{\xi-5}{\xi-1}\frac{\Gamma(\xi-2)\Gamma\left(\frac{5-\xi}{2}\right)}{\Gamma^3\left(\frac{\xi-1}{2}\right)}\right)^{\frac{1}{5-\xi}}, \qquad (38)$$

compare the black and gray dotted curves with the red and pink dashed curves in the figure. If $Z^{5-\xi} \gg 1$, which is true for $\xi = 3.9$, then κ_L is proportional to Z^{-1}, i.e., to w_{max}^{-1} (see Eq. (38)). At the frequencies $k_\perp \gg w_{max}^{-1}$, the product $(< w^2 > PSD2_\Theta)$ does not depend on Z – the gray and black dotted curves in Fig. 3 coincide. Since the low frequencies $k_\perp \leqslant w_{max}^{-1}$ contribute only to contrast at small times (see Section 2), Z affects the contrast only slightly.

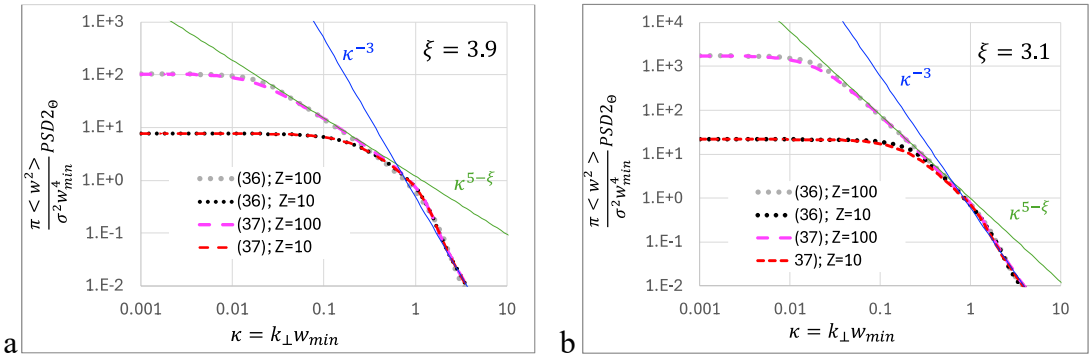

Fig. 3. $PSD2_\Theta$ normalized to $\frac{\sigma^2 w_{min}^4}{\pi < w^2 >}$ as a function of $\kappa = k_\perp w_{min}$ for $\xi = 3.9$ (a) and $\xi = 3.1$ (b). Dotted curves – exact Eq. (36) for Z=100 (gray) and Z=10 (black); dashed curves – approximate Eq. (37) for Z=100 (pink) and Z=10 (red).

4. PSD functional form PSD_r for roughness of the grating/mirror surface

The surface profile $h(\boldsymbol{r})$ is characterized by the function $PSD2_h(k_\perp)$ related to the power spectral density of the introduced phase fluctuations $PSD2_r(k_\perp)$ by

$$PSD2_r(k_\perp) = B_0 k_o^2 PSD2_h(k_\perp) , \qquad (39)$$

where $B_0 = (cos\alpha + cos\beta)^2$ for the grating [50] and $B_0 = 4cos^2\alpha$ for the mirror. Much attention in the literature has been paid to measuring $PSD1_h(k_x)$ [5, 11, 14, 19, 23, 45, 51-55]. In general, it behaves differently in different spectral ranges for different optical elements. In such a case, it is necessary to substitute the experimental data into Eqs. (39, 27) and the result into Eq. (25). At medium and high spatial frequencies, $PSD2_h$ often has a power-law form, and at low frequencies it is equal to a constant. Therefore, $PSD2_h$ is well approximated by a Lorentz-type spectrum [21, 45, 56] with correlation length $1/k_h$, surface profile dispersion σ_h^2, and exponent $a > 2$. Then

$$PSD2_r(k_\perp) = \frac{a-2}{2\pi}\sigma_h^2 B_0 k_0^2 \frac{k_h^{a-2}}{(k_h^2+k_\perp^2)^{a/2}} \qquad PSD1_r(k_x) = \frac{\Gamma\left(\frac{a-1}{2}\right)}{\sqrt{\pi}\Gamma\left(\frac{a-2}{2}\right)}\sigma_h^2 B_0 k_0^2 \frac{k_h^{a-2}}{(k_h^2+k_x^2)^{(a-1)/2}} \qquad (40)$$

Usually, $2 < a < 4$. A frequently encountered value is $a \approx 2.55$, including in the work [54], where $PSD1_h(k_\perp)$ was measured for an off-axis parabola used for writing holographic gratings.

5. *PSD* functional form for obscuration and roughness of the optics used for writing gratings

When writing a holographic grating, even with a perfectly plane substrate surface, the grating is not ideal due to the non-equidistance and non-parallelism of the grooves, as well as due to groove profile fluctuations.

The non-equidistance and non-parallelism of the grooves are determined by spatial fluctuations in the phase difference of two writing beams and give rise to fluctuations in the phase of the beam reflected from the grating $\Delta\varphi(\boldsymbol{r}) \neq 0$ [25-28], without affecting the reflection

https://doi.org/10.1017/hpl.2025.10073 Published online by Cambridge University Press

coefficient: $\mathcal{A}(\boldsymbol{r}) = 0$. For a holographic grating this phase is equal to the phase of the writing field ϕ_{wr} scaled along the *x* axis [27]: $\Delta\varphi(\boldsymbol{r}) = \phi_{wr}(xcos\Phi, y)$. Here, Φ is the angle of incidence on the substrate (Fig. 4), $sin\Phi = N\lambda_{wr}/2$. The phase $\Delta\varphi(\boldsymbol{r})$ is added to the phase $\varphi(\boldsymbol{r})$ associated with the non-flat surface of the grating that was discussed in Section 4. Since these phases are uncorrelated, their *PSD*s are summed. Considering that $cos\Phi$ is usually close to unity, we will assume that the *PSD* functions for $\Delta\varphi$ and ϕ_{wr} are equal and designate them as $PSD2_{phase}$.

The fluctuations in the groove shape are caused by spatial fluctuations in the intensity of the radiation used to write the grating and give rise to the fluctuations in the modulus of the grating reflectivity $\mathcal{A}(\boldsymbol{r}) \neq 0$ [24], without affecting its phase: $\Delta\varphi(\boldsymbol{r}) = 0$. Rigorous calculation of the *PSD* of the grating reflectivity fluctuations $PSD2_a$ is a complex problem that requires knowledge of exact relationship between these fluctuations and the intensity fluctuations of the writing field $|E_{wr}(\boldsymbol{r})|^2$. However, taking into account the smallness of both fluctuations relative to their mean values, we will assume that they are proportional to each other. Then $PSD2_a = qPSD2_{dose}$, where $q > 0$ is a dimensionless coefficient, and $PSD2_{dose}$ is $PSD2$ for the radiation intensity on the substrate normalized to the average value. Now we need to find $PSD2_{phase}$ and $PSD2_{dose}$.

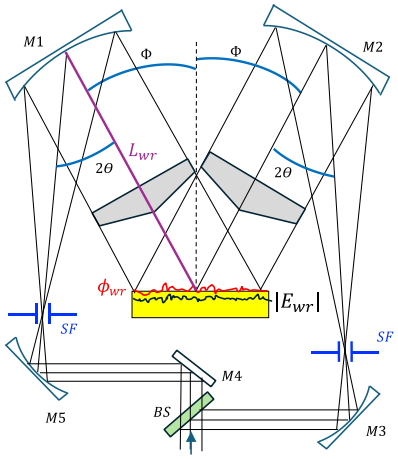

Fig. 4. Scheme of writing holographic diffraction grating by two laser beams. BS – beamsplitter, M1-M5 – mirrors, and SF – spatial filters.

Since all dynamic noises are averaged during grating exposure, only the "frozen" noises caused by the imperfection of the transport optics are significant. Obviously, the fewer optical elements are used, the better. A scheme for writing a holographic grating that is optimal from this point of view is presented in Fig. 4 [54]. Since the spatial filter ensures good filtering of high-frequency noise, only the transport optics located after the filters is of fundamental importance. The scheme in Fig. 4 contains a minimum number of such elements – two off-axis parabolic mirrors (OAP). In the classical work [57] and other [24] papers, collimators are additionally used, which increases fluctuations. When reflecting the beam $E_{wr}(\boldsymbol{r})$ these two OAPs introduce into it both the amplitude noise caused by scratches and defects (obscuration), and the phase noise caused by the imperfection/roughness of the surface. Let us denote by $PSD2_{m,\Theta}$ and $PSD2_{m,\varphi}$ the power spectral density of the amplitude and phase of the field reflected from the OAP. We assume that the statistical properties of the OAP surface are the same as the properties of the grating surface, i.e., they have equal $PSD2_h(k_\perp)$. Then $PSD2_{m,\varphi} = \frac{B_{wr}k_{wr}^2}{B_0k_0^2}PSD2_r$, Eq. (40), where k_{wr} is the wave vector of the writing radiation and $B_{wr} = 4cos^2\theta$, where θ is the angle of incidence on the OAP (Fig. 4). Analogously, we assume that the statistical properties of obscuration on these mirrors are the same as on the gratings, i.e., $PSD2_{m,\Theta} = \frac{\sigma_{wr}^2}{\sigma_\Theta^2}PSD2_{ob}$, Eq. (37). For unused gratings it is reasonable to assume that $\sigma_\Theta^2 = \sigma_{wr}^2$, but with long-term use of gratings in high-power radiation the number of defects increases and $\sigma_\Theta^2 \gg \sigma_{wr}^2$, see Section 3.

https://doi.org/10.1017/hpl.2025.10073 Published online by Cambridge University Press

The field on the substrate differs from the field on the mirror, since when the light is propagating from the mirror to the substrate over distance L_{wr}, the fluctuations of the amplitude and phase of the field transform into each other. An expression for $PSD2_{dose}$ when a beam propagates in free space was obtained in [44], from which, in the particular case of monochromatic radiation of interests to us, we find

$$PSD2_{dose} = 4T\left(PSD2_{m,\Theta} + PSD2_{m,\varphi}\right) + 4Re\left(T_2 e^{iL_{wr}k_\perp^2/k_0}\right)\left(PSD2_{m,\Theta} - PSD2_{m,\varphi}\right), \quad (41)$$

where

$$T(\boldsymbol{\rho}) = \frac{\int |E_{wr}(\boldsymbol{r})|^2 |E_{wr}(\boldsymbol{r}-\boldsymbol{\rho})|^2 \boldsymbol{dr}}{\int |E_{wr}(\boldsymbol{r})|^4 \boldsymbol{dr}} \qquad T_2(\boldsymbol{\rho}) = \frac{\int E_{wr}^*(\boldsymbol{r}-\boldsymbol{\rho}) E_{wr}^*(\boldsymbol{r}+\boldsymbol{\rho}) E_{wr}^2(\boldsymbol{r}) \boldsymbol{dr}}{\int |E_{wr}(\boldsymbol{r})|^4 \boldsymbol{dr}} \qquad \boldsymbol{\rho} = L_{wr}\boldsymbol{k}_\perp/k_0. \quad (42)$$

Here, we took into account that two OAPs with uncorrelated noises contribute to $PSD2_{dose}$, i.e., the $PSD2_{dose}$ Eq. (41) is twice as large as that for one beam reported in [44]. It can be readily shown that the PSD of field amplitude fluctuations $|E_{wr}(\boldsymbol{r})|$ is 4 times smaller than the $PSD2_{dose}$ and the sum of the PSD of the field amplitude fluctuations $|E_{wr}(\boldsymbol{r})|$ and the PSD of the field phase $\phi_{wr}(\boldsymbol{r})$ is $4T\left(PSD2_{m,\Theta} + PSD2_{m,r}\right)$. Thus, $PSD2_{phase} = \frac{1}{4}PSD2_{dose}$.

The authors of [54] derived an expression similar to Eq. (41) with $T = 1$, i.e., neglecting the finite beam aperture $E_{wr}(\boldsymbol{r})$ (see below). The term with T_2 corresponds to the Talbot effect. Considering that L_{wr} is on the order of 10 meters, at large $k_\perp$ this term rapidly oscillates around zero. In addition, since the contribution to $PSD2_{phase,dose}$ is made by two surfaces with close but not identical distances L_{wr}, the total phase fluctuations at large $k_\perp$ are averaged. Therefore, this term can be approximately replaced by its average value, which is obviously equal to zero, i.e., we can set $T_2 = 0$. The function $T(\boldsymbol{\rho})$ corresponds to the spatial self-filtering of noise during propagation in free space [44, 58, 59], which is associated with the fact that part of the high-frequency noise escapes from the beam aperture. The transmittance $T(\boldsymbol{\rho})$, that is the normalized ACF of the writing beam intensity, is close to unity at $\rho \ll R_0$, i.e., for $\frac{L_{wr}}{R_0} \ll \frac{k_0}{k_\perp}$. Since $L_{wr} \approx 10R_0$, then $T(\boldsymbol{\rho}) \approx 1$ for $k_\perp \ll 0.1k_0$. This condition is more rigorous than the paraxial approximation condition $k_\perp \ll k_0$, so self-filtering cannot be completely neglected. At the same time, $T(\rho = R_0) \approx 1/2$, i.e., for $k_\perp = 0.1k_0$ (the paraxial approximation boundary), the error will be about two. Therefore, assuming $T(\boldsymbol{\rho}) \approx 1$ we obtain a slightly overestimated noise value at high ($k_\perp \approx 0.1k_0$) frequencies and, consequently, a slightly overestimated contrast value at large times. From Eq. (41), with $T = 1$ and $T_2 = 0$ taken into account, we have

$$PSD2_{phase} = \frac{\sigma_{wr}^2}{\sigma_\Theta^2} PSD2_\Theta + \frac{B_{wr}k_{wr}^2}{B_0 k_0^2} PSD2_r \qquad PSD2_{dose} = 4PSD2_{phase}, \quad (43)$$

where $PSD2_\Theta$ is defined by Eqs. (37, 36), and $PSD2_r$ by Eq. (40). Taking into account the linear relationship of $PSD1$ and $PSD2$ Eq. (27), an expression for $PSD1$ is analogous to Eq. (43). The results presented in Sections 3–5 are summarized in Table 1, from which we obtain the final expression for the total PSD for one grating:

$$PSD2 = \left(1 + \{1 + 4q\}\frac{\sigma_{wr}^2}{\sigma_\Theta^2}\right) PSD2_\Theta + \left(1 + \{1 + 4q\}\frac{B_{wr}k_{wr}^2}{B_0 k_0^2}\right) PSD2_r \quad (44)$$

By substituting Eq. (44) into Eq. (26) we obtain an expression for the contrast $\mathbb{C}_s(t)$ for gratings G2 and G3, and the substitution of Eq. (44) into Eq. (29) gives an expression for the contrast $\mathbb{C}_d(t)$ for gratings G1 and G4, as well as for the mirrors on the input and output optics. Note that for the mirrors the expressions in parentheses in Eq. (44) should be replaced by 1, since in this work we neglect fluctuations in the mirror reflectivity.

https://doi.org/10.1017/hpl.2025.10073 Published online by Cambridge University Press

Table 1. PSD for one grating (for a mirror, the columns "writing" would contain zeros)

	Obscurations		Roughness	
	beamline	writing	beamline	writing
Amplitude fluctuations $PSD2_\Theta(\boldsymbol{k}_\perp) + PSD2_a(\boldsymbol{k}_\perp)$	PSD_Θ Eq. (37) (exact Eq. (36))	$4q\frac{\sigma_{wr}^2}{\sigma_\Theta^2}PSD_\Theta$	---	$4q\frac{B_{wr}k_{wr}^2}{B_0k_0^2}PSD_r$
Phase fluctuations $PSD2_\varphi(\boldsymbol{k}_\perp)$	---	$\frac{\sigma_{wr}^2}{\sigma_\Theta^2}PSD_\Theta$	PSD_r Eq. (40)	$\frac{B_{wr}k_{wr}^2}{B_0k_0^2}PSD_r$

6. Example of contrast $\mathbb{C}(t)$ calculations

Above we considered the contrast introduced by one of the optical elements shown in Fig. 1. In what follows we will assume that the total contrast is equal to the sum of the contrasts introduced by each element. This is obvious for obscurations and surface imperfections (both of the grating and of the mirror), since the obscurations are randomly located on different elements and the $\Theta(\boldsymbol{r})$ functions of different elements are uncorrelated. The same applies to the roughness of beamline optics. For the contrast associated with writing the gratings, the issue is more complicated. It is reasonable to assume that all gratings are written under the same conditions; then their functions $\mathcal{A}(\boldsymbol{r})$ and $\Delta\varphi(\boldsymbol{r})$ are correlated. A strong correlation for $\Delta\varphi(\boldsymbol{r})$ was measured in [28]. However, since G2 and G3 (as well as G1 and G4) are mirror-like in the compressor, their identity is lost by virtue of the uncorrelated $\mathcal{A}(x,y)$ and $\mathcal{A}(-x,y)$. For definiteness, we will assume that both the input and output optics consist of four mirrors. We will use the geometric parameters of the compressor from the XCELS project [43], see Table 2.

Table 2. Compressor parameters

λ_0, nm	910		t_p, fs	20
A	0.97		τ_x, ns	3.07
E=F	3.55		t_c for $G2$, ps	249
K=G	0		t_c for $G2$, ps	338
L, m	1.9		$t_{xy} = \tau_y$	0
$L_{in} = L_{out}$, m	5		$t_x = t_y = t_d$ for G2, ns	37.9
L_{23}, m	6		$t_x = t_y = t_d$ for G3, ns	27.9
L_p, m	5			

We have neither theoretical nor experimental data on the value of q, but we can make the following estimate. For the dispersion of the power reflectivity of the grating $\sigma_R^2 = 2\sigma_a^2$, we obtain $\sigma_R^2 = 8q\sigma_h^2 B_{wr}k_{wr}^2$. We will take the minimum value of σ_h available in the literature, which at $k_h = 0.1/\text{mm}$ is $\sigma_h = 0.38$ nm [54]. Then at $\lambda_{wr} = 413$ nm, $B_{wr} = 3.7$, and $q = 1$ we obtain $\sigma_R = 0.03$, which is an unreasonably large value for such high-quality optics. For the NIF standard optics, $\sigma_h = 3.8$ nm and $\sigma_R = 0.03$ is obtained at $q = 0.01$. Although these estimates are very rough, we can conclude from them that $q \ll 0.1$ and set $q = 0$ in Eq. (44). In other words, the impact of the writing optics imperfections on the fluctuations of the grating reflectivity may be neglected and only the diffracted wave phase fluctuations will be taken into account.

The solid curves in Fig. 5 show the *PCR* introduced by gratings G2 and G3, and the dotted curves show the *PCR* introduced by all the other optical elements taken together: gratings G1 and G4, as well as the input M_{in} and output M_{out} optics. As stated above, such a partitioning is made because only gratings G2 and G3 have a spatial chirp ($\tau_x \neq 0$) and it is necessary to use either the exact Eq. (25) or the approximate Eq. (26), from which it follows that the cut-off time t_c Eq. (22) is 249 ps for G3 and 338 ps for G2, i.e., there are both a pre-pulse and a post-pulse. There is no

https://doi.org/10.1017/hpl.2025.10073 Published online by Cambridge University Press

spatial chirp ($\tau_x = 0$) on all the other elements, so one can use Eq. (29), from which it follows that the cut-off time is zero, i.e., there is no pre-pulse (if there is no negative diffraction, see Section 2).

The red and blue curves in Fig. 5 correspond to the contrast $\mathbb{C}_{ob}(t)$ caused by obscurations and the contrast $\mathbb{C}_r(t)$ caused by surface roughness. To obtain $\mathbb{C}_{ob}(t)$, only the first term from Eq. (44) (i.e., the term with $PSD2_\Theta$ from Eq. (37)) should be substituted into Eqs. (25, 29). The analysis shows that $\mathbb{C}_{ob}(t)$ is almost independent of *Z,* it depends only on two dimensionless quantities – ξ and $k_0 w_{min}$. Further, we will assume that $w_{min} = 0.25$ mm, $\xi = 3.9$ [23] and that the compressor has already been used in a large number of shots, as a result of which grating G4 and the output optics "accumulated" obscurations in the amount measured in [23], which corresponds to $\sigma_\Theta^2 = 6.1 \cdot 10^{-4}$. The input optics, gratings G1–G3 and writing optics are not exposed to powerful femtosecond radiation, so we will assume that for them $\sigma_\Theta^2 = 6.1 \cdot 10^{-6}$, i.e., it is 100 times smaller. We remind the reader that σ_Θ^2 is equal to the fraction of the surface occupied by obscurations, as well as to the fraction of the noise energy W_Θ/W_0, see Section 2.

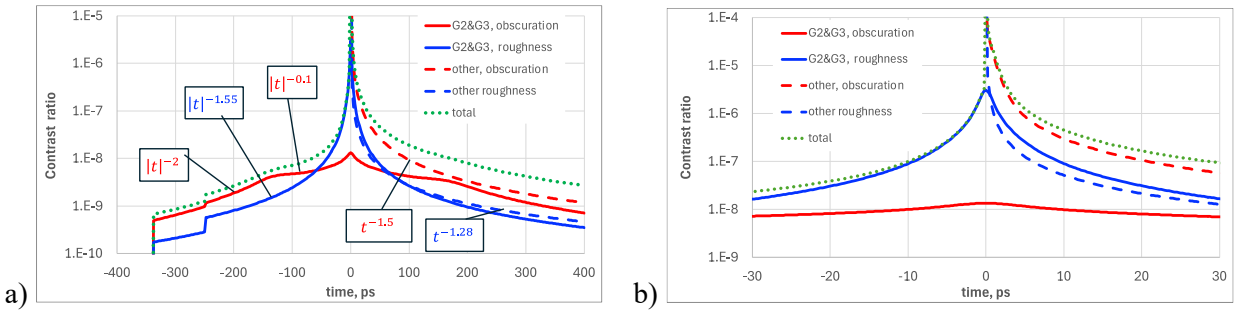

Fig. 5. Contrast $\mathbb{C}_{ob}(t)$ (red) and $\mathbb{C}_r(t)$ (blue) for gratings G2 and G3 (solid curves), for other optical elements (dashed curves), and total contrast for the entire compressor (green dotted curve). (a) and (b) differ only by the scale of the horizontal axis.

To obtain $\mathbb{C}_r(t)$, it is necessary to substitute into Eqs. (25, 29) only the second term from Eq. (44) (the term with $PSD2_r$ from Eq. (40)). The analysis of these expressions shows that $\mathbb{C}_r(t)$ depends only on two dimensionless quantities – a and $\sigma_r^2 = B_0 k_0^2 \sigma_h^2 (k_h/k_0)^{a-2}$, with the dependence on σ_r^2 being linear. In other words, for a fixed *a,* the shape of $\mathbb{C}_r(t)$ does not change. Further, we will assume that $a = 2.55$, and σ_h^2 of all optical elements, including mirrors used for writing the gratings (see Fig. 4), is 200 times less than the data in [55], 10 times less than the NIF standard [23], but 10 times more than the data reported in [54]. At $k_h = 0.1/\text{mm}$ this corresponds to $\sigma_h \approx 1.2$ nm. It is easy to show that the fraction of the noise energy $\sigma_\varphi^2 = W_\varphi/W_0$ caused by scattering on a rough surface is equal to $\sigma_h^2 B_0 k_0^2$ and at $B_0 = 2.8$ we obtain $\sigma_\varphi^2 \approx 1.9 \cdot 10^{-4}$. This is approximately 30 times more than $\sigma_\Theta^2 = 6.1 \cdot 10^{-6}$ presented above. However, at large times $\mathbb{C}_r \ll \mathbb{C}_{ob}$, since $\mathbb{C}_{ob}$ decreases very slowly. As a result, at large times the total *PCR* is determined by $\mathbb{C}_{ob}$, and at small times by $\mathbb{C}_r$. This qualitative conclusion is valid for a wide range of σ_φ^2 and σ_Θ^2. Any quantitative comparison of $\mathbb{C}_{ob}$ and $\mathbb{C}_r$ strongly depends on the quality of the optical elements, because $\mathbb{C}_{ob,r}$ are proportional to $\sigma_{\Theta,\varphi}^2$ and the $\sigma_\varphi^2/\sigma_\Theta^2$ ratio can vary over a wide range in practice. For example, the boundary is the instant of time at which $\mathbb{C}_r = \mathbb{C}_{ob}$ is $t_* = -60ps$ in Fig.5a. If the optics roughness σ_φ^2 increases by a factor of 10, $\mathbb{C}_r$ also increases by a factor of 10 and $t_* = -12ps$.

The small deviation of the contrast from parity observed in Fig. 5 for curves G2 and G3 constructed according to Eq. (25) may be neglected in practice and a simpler Eq. (26) can be used instead of Eq. (25), i.e., $\mathbb{C}(t)$ is proportional to $PSD1(k_x)$ and the mapping is linear: $t = \tau_x k_x/k_0$. Since in the focal plane the distance from the beam axis (along the *x* axis) is $x = Fk_x/k_0$, then for the pre-pulse, x is related to the time of its appearance on the target as $x = Ft/\tau_x$. Thus, the radiation reaches the target at the time $t = -t_c$, illuminating a vertical strip at a distance $x = Ft_c/\tau_x$, see Fig. 6a. Then this strip splits into two and its replicas move in opposite directions at

https://doi.org/10.1017/hpl.2025.10073 Published online by Cambridge University Press

speed F/τ_x. At $t = 0$, one of them reaches the axis and continues to move in the same direction at the same speed. The intensity, and hence, the fluence change proportionally to $\mathbb{C}(t)$. For any given fluence value (for example, at which the target is destroyed), this simple reasoning allows us to calculate for each point of the target the time at which this value will be reached.

For all the other optical elements, except for G2 and G3, PCR $\mathbb{C}(t)$ is proportional to $PSD2(k_\perp)$ Eq. (29) and the mapping is quadratic: $t = t_d k_\perp^2/k_0^2$. The radiation reaches the target at $t = 0$, exactly at the beam axis. At all subsequent instants of time, the radiation illuminates a ring of radius $r = Fk_\perp/k_0 = F\sqrt{t/t_d}$, which increases in proportion to $\sqrt{t}$ (Fig. 6b).

The laws of $\mathbb{C}(t)$ degrease are different, see Fig. 5a. The $\mathbb{C}_{ob}(t)$ curve for G2 and G3 clearly features the boundary between the two ranges, in which the law of $\mathbb{C}_{ob}(t)$ degrease changes from $|t|^{-0.1}$ to $|t|^{-2}$. Unfortunately, quantitative comparison with the experiments is impossible for lack of PSD functions for the gratings and optics used in the experiments. There is a good qualitative agreement between $\mathbb{C}_{ob}(t)$ and the results of measurements [11], where a plateau (an area where $\mathbb{C}_{ob}(t) \sim |t|^{-0.1}$) caused by scattering at stretcher mirrors, which is equivalent to scattering at gratings G2 and G3 [22], was also observed. The theory (in particular the dotted curve in Fig.5) explains the frequently observed experimental asymmetry of the contrast: the post-pulse is larger than the pre-pulse [5, 15-18, 46, 47]. Also, Figure 5a shows typical "triangular" $\mathbb{C}(t)$ shapes observed in many experiments [5, 8, 11, 14-19, 47].

Despite the larger number of elements (two gratings and 8 mirrors), the $\mathbb{C}_r(t)$ for G2 and G3 is close to $\mathbb{C}_r(t)$ for all the other elements. The point is that the contribution of $\mathbb{C}_r(t)$ for gratings is much larger than for mirrors, since in mirrors there is no dominant (due to $k_{wr}^2 \gg k_0^2$) contribution from writing optics.

For the PCR caused by the roughness of gratings and mirrors of the input and output optics, generalizations to advanced compressors and stretcher were proposed in [22]. Without repeating them here, we just note that they are valid for all the results obtained above, since they are based on the expression (19) in [22], which coincides with Eq. (17) if $PSD2_\varphi(\boldsymbol{k}_\perp)$ is replaced by $PSD2(\boldsymbol{k}_\perp)$.

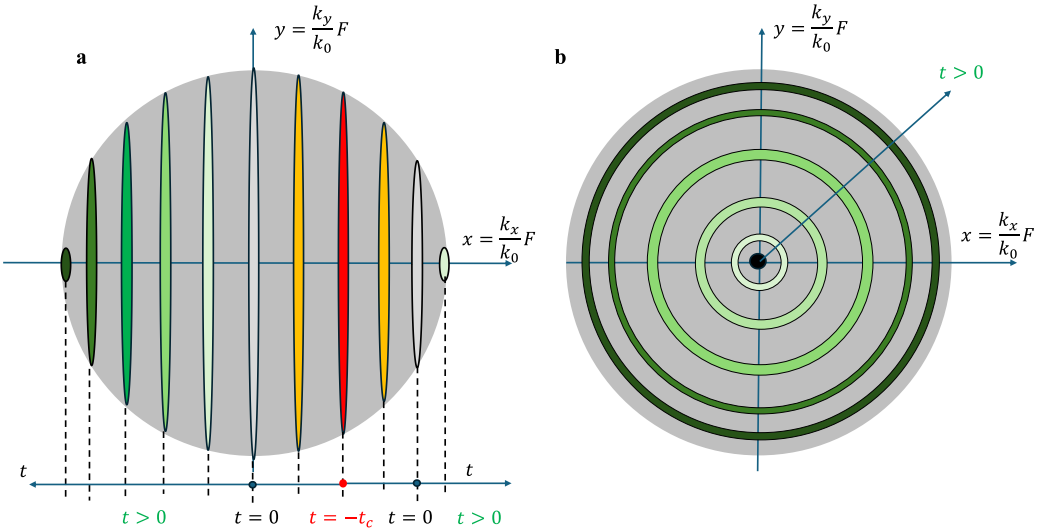

Fig. 6. Schematic representation of the target illumination dynamics in the focal plane. a) For gratings G2 and G3, b) for all other optical elements depicted in Fig. 1.

7. Conclusion

In the paraxial approximation, with allowance for all orders of dispersion, the problem of the impact of imperfect compressor gratings and transport optics on the PCR $\mathbb{C}(t)$ Eq. (1) of a femtosecond laser pulse has been solved. All types of imperfections have been considered: non-flat surface profile (roughness), dirt/damage/obscuration on the surface, as well as roughness and obscuration on the optics used to write holographic gratings. The analytically obtained Eq. (25)

https://doi.org/10.1017/hpl.2025.10073 Published online by Cambridge University Press

for $\mathbb{C}(t)$ is valid for any optical element, for both the Treacy compressor and the out-of-plane compressor. For finding $\mathbb{C}(t)$ it is sufficient to know the *PSD* of the field reflected from an imperfect optical element. For the roughness, the field *PSD* is determined by the *PSD* of the surface profile and for the obscuration, by the obtained Eq. (36).

Strictly speaking, the *PCR* caused by the imperfections of the second and third gratings is not an even function of time, since diffraction results in the cutoff time t_c: $\mathbb{C}(t < -t_c) = 0$, as well as in a small deviation from parity at $|t| < t_c$. However, this deviation is small and can be neglected in practice. Then $\mathbb{C}(t)$ is proportional to $PSD1(k_x)$ of the reflected field Eq. (26), with the arguments of these functions being related linearly as $t = \tau_x k_x/k_0$. The radiation scattered by the second and third gratings arrives at the target at the time $t = -t_c$, illuminating a vertical stripe at the distance $x = Ft_c/\tau_x$ (Fig. 6a). Then this stripe bifurcates and its replicas move in opposite directions at a speed F/τ_x. One of them, at the time of the main pulse arrival $(t = 0)$, reaches the beam axis and continues to move in the same direction at the same speed.

The PCR caused by imperfections of all the other optical elements, except for the second and third gratings, is nonzero only at $t > 0$. This radiation reaches the target at $t = 0$ exactly on the beam axis and further moves away from the axis like a circle on water from a thrown stone. $\mathbb{C}(t)$ is proportional to the $PSD2(k_\perp)$ of the reflected field Eq. (29), with the arguments of these functions being related quadratically: $t = t_d k_\perp^2/k_0^2$. It is the scattering on other optical elements that explains the contrast asymmetry observed in the experiment when the sign of the time is changed.

With the same roughness and the same obscuration, the contribution to the PCR of the optics used to write holographic gratings is significantly greater than the contribution of the gratings themselves. This is due to the fact that shorter-wave radiation is used for writing, and the phase distortions are proportional to λ^{-1}.

The comparison of $\mathbb{C}_{ob}(t)$ caused by obscurations and $\mathbb{C}_r(t)$ caused by roughness shows that, at small t, $\mathbb{C}_r(t)$ prevails and at large t, $\mathbb{C}_{ob}(t)$, since its distinctive feature is a very slow decrease with increasing $|t|$ (Fig. 5a). The instant of time at which $\mathbb{C}_{ob}(t) = \mathbb{C}_r(t)$ strongly depends on the proportion of the radiation power scattered on obscuration and on roughness.

Funding

Ministry of Science and Higher Education of the Russian Federation (Project No. FFUF-2024-0038).

References

1. Z. Li, Y. Leng, and R. Li, "Further development of the short-pulse Petawatt laser: trends, technologies, and bottlenecks", Laser & Photonics Review **7**, 2100705 (2022) 10.1002/lpor.202100705.
2. C. Dorrer, "Spatiotemporal metrology of broadband optical pulses", IEEE Journal of Selected Topics in Quantum Electronics **25**, 3100216 (2019) 10.1109/JSTQE.2019.2899019.
3. A. Jeandet, S. Jolly, A. Borot, B. Bussière, P. Dumont, J. Gautier, O. Gobert, J.-P. Goddet, A. Gonsalves, A. Irman, W. Leemans, R. B. Lopez-Martens, G. Mennerat, K. Nakamura, M. Ouillé, G. Pariente, M. Pittman, T. Püschel, F. Sanson, F. Sylla, C. Thaury, K. Zeil, and F. Quéré, "Survey of spatio-temporal couplings throughout high-power ultrashort lasers", Optics Express **30**, 3263-3288 (2022) 10.1364/oe.444564.
4. V. Bagnoud and F. Salin, "Influence of optical quality on chirped-pulse amplification: characterization of a 150-nm-bandwidth stretcher", J. Opt. Soc. Am. B **16**, 188-193 (1999) •https://doi.org/10.1364/JOSAB.16.000188.

https://doi.org/10.1017/hpl.2025.10073 Published online by Cambridge University Press

5. B. Webb, C. Dorrer, S.-W. Bahk, C. Jeon, R. G. Roides, and J. Bromage, "Temporal contrast degradation from mid-spatial-frequency surface error on stretcher mirrors", Applied Optics **63**, 4615-4621 (2024) https://doi.org/10.1364/AO.522892.
6. X. Xie, J. Zhu, P. Zhu, M. Sun, Q. Yang, H. Zhu, A. Guo, J. Kang, and Q. Gao, "On target contrast ratio study for petawatt level femtosecond laser system," in *Short-pulse High-energy Lasers and Ultrafast Optical Technologies*, 2019), 110340H, https://doi.org/10.1117/12.2520821.
7. W. Li, X. Wang, Y. Zuo, Y. Hong, B. Hu, Z. Wu, J. Mu, K. Zhou, and X. Zeng, "A cylindrical Öffner stretcher based on ternary reflector for femtosecond petawatt-level laser system", Chinese Optics Letters **21**, 073201 (2023) 10.3788/COL202321.073201.
8. V. A. Schanz, M. Roth, and V. Bagnoud, "Picosecond contrast degradation by surface imperfections in chirped-pulse-amplification stretchers", Journal of the Optical Society of America A **36**, 1735-1742 (2019) https://doi.org/10.1364/JOSAA.36.001735.
9. Z. Li, N. Miyanaga, and J. Kawanaka, "Theoretical comparison of spatiotemporal contrasts of pulsed beams in unfocusing, 1D-focusing, and 2D-focusing fields and enhancement of the on-axis temporal contrast at the focus", Journal of the Optical Society of America B **35**, 1861-1870 (2018) •https://doi.org/10.1364/JOSAB.35.001861.
10. Z. Li, S. Tokita, S. Matsuo, K. Sueda, T. Kurita, T. Kawasima, and N. Miyanaga, "Scattering pulse-induced temporal contrast degradation in chirped-pulse amplification lasers", Optics Express **25**, 21201-21215 (2017) •https://doi.org/10.1364/OE.25.021201.
11. S. Roeder, Y. Zobus, Z. Major, and V. Bagnoud, "Improving the rising edge of the temporal contrast of PHELIX by spatial conditioning in an unfolded stretcher", Optics Express **32**, 35713-35724 (2024) https://doi.org/10.1364/OE.519252.
12. P. Zhu, X. Xie, X. Ouyang, and J. Zhu, "Output temporal contrast simulation of a large aperture high power short pulse laser system", High Power Laser Science and Engineering **2**, e42 (2014) https://doi.org/10.1017/hpl.2014.47.
13. H. Kiriyama, Y. Mashiba, Y. Miyasaka, and M. R. Asakawa, "Random spectral phase noise effect on the temporal contrast of ultra-high intensity laser pulse", Review of Laser Engineering **46**, 142-144 (2018) 10.2184/lsj.46.3_142.
14. L. Ranc, C. Blanc, N. Lebas, L. Martin, J.-P. Zou, F. Mathieu, C. Radier, S. Ricaud, F. Druon, and D. Papadopoulos, "Improvement in the temporal contrast in the tens of ps range of the multi-PW Apollon laser front-end", Optics Letters **45**, 4599-4602 (2020) •https://doi.org/10.1364/OL.401272.
15. C. Hooker, Y. Tang, O. Chekhlov, J. Collier, E. Divall, K. Ertel, S. Hawkes, B. Parry, and P. P. Rajeev, "Improving coherent contrast of petawatt laser pulses", Optics Express **19**, 2193-2203 (2011)
16. Y. Tang, C. Hooker, O. Chekhlov, S. Hawkes, J. Collier, and P. P. Rajeev, "Transmission grating stretcher for contrast enhancement of high power lasers", Optics Express **22**, 29363-29374 (2014) DOI:10.1364/OE.22.029363.
17. H. Kiriyama, Y. Miyasaka, A. Kon, M. Nishiuchi, A. Sagisaka, H. Sasao, A. S. Pirozhkov, Y. Fukuda, K. Ogura, K. Kondo, N. Nakanii, Y. Mashiba, N. P. Dover, L. Chang, M. Kando, S. Bock, S. Ziegler, T. Püschel, H.-P. Schlenvoigt, K. Zeil, and U. Schramm, "Laser output performance and temporal quality enhancement at the J-KAREN-P Petawatt laser facility", Photonics **10**, 997 (2023) doi.org/10.3390/photonics10090997.
18. X. Lu, H. Zhang, J. Li, and Y. Leng, "Reducing temporal pedestal in a Ti:sapphire chirped-pulse amplification system by using a stretcher based on two concave

https://doi.org/10.1017/hpl.2025.10073 Published online by Cambridge University Press

mirrors", Optics Letters **46**, 5320-5323 (2021) •https://doi.org/10.1364/OL.435145.
19. S. Roeder, Y. Zobus, C. Brabetz, and V. Bagnoud, "How the laser beam size conditions the temporal contrast in pulse stretchers of chirped-pulse amplification lasers", High Power Laser Science and Engineering **10**, e34 (2022) doi:10.1017/hpl.2022.18.
20. C. Dorrer and J. Bromage, "Impact of high-frequency spectral phase modulation on the temporal profile of short optical pulses", Optics Express **16**, 3058-3068 (2008)
21. J. Bromage, C. Dorrer, and R. K. Jungquist, "Temporal contrast degradation at the focus of ultrafast pulses from high-frequency spectral phase modulation", JOSA B **29**, 1125-1135 (2012) •https://doi.org/10.1364/JOSAB.29.001125.
22. E. Khazanov, "Analytical dependence of time contrast ratio on surface imperfection of optics in femtosecond lasers", Opt. Express, accepted (2025) https://doi.org/10.1364/OE.558639.
23. M. L. Spaeth, K. R. Manes, C. C. Widmayer, W. H. Williams, P. K. Whitman, M. A. Henesian, I. F. Stowers, and J. Honig, "National ignition facility wavefront requirements and optical architecture", Optical Engineering **43**, 2854-2865 (2004) https://doi.org/10.1117/1.1815332.
24. F. Koch, D. Lehr, and T. Glaser, "Stability requirements for two-beam interference lithography diffraction grating manufacturing," in *SPIE Optifab*, (SPIE, 2017), 104481L-104481, 10.1117/12.2277007.
25. F. Bienert, C. Röcker, T. Dietrich, T. Graf, and M. A. Ahmed, "Detrimental effects of period-chirped gratings in pulse compressors", Optics Express **31**, 40687-40704 (2023) https://doi.org/10.1364/OE.505875.
26. N. Bonod and J. Neauport, "Diffraction gratings: from principles to applications in high-intensity lasers", Advances in Optics and Photonics **8**, 156-199 (2016) •https://doi.org/10.1364/AOP.8.000156.
27. E. Khazanov, "Wavefront distortions of a laser beam reflected from a diffraction grating with imperfect surface and groove pattern ", Optics Express **32**, 46310 (2024) https://doi.org/10.1364/OE.542565.
28. A. Kochetkov, A. Shaykin, I. Yakovlev, E. Khazanov, A. Cheplakov, B. Wang, Y. Jin, S. Liu, and J. Shao, "Precise characterization of diffraction grating groove pattern", Opt. Express **33**, 13673-13681 (2025) doi.org/10.1364/OE.551097.
29. E. B. Treacy, "Optical pulse compression with diffraction gratings", IEEE Journal of Quantum Electronics **QE-5**, 454-458 (1969)
30. K. Osvay and I. N. Ross, "On a pulse compressor with gratings having arbitrary orientation", Optics Communications **105**, 271-278 (1994)
31. E. Khazanov, "New grating compressor designs for XCELS and SEL-100 PW projects", High Power Laser Science and Engineering **12**, e36 (2024) 10.1017/hpl.2024.18.
32. A. Vyatkin and E. Khazanov, "Grating compressor optimization aiming at maximum focal intensity of femtosecond laser pulses", Optics Express **32**, 39394-39407 (2024) •https://doi.org/10.1364/OE.535150.
33. E. Khazanov, "Impact of beam clipping in full-aperture grating compressors on focal intensity contrast ratio", JOSA B **42**, 1423-1429 (2025) doi.org/10.1364/JOSAB.563342.
34. E. Khazanov, "Reducing laser beam fluence and intensity fluctuations in symmetric and asymmetric compressors", High Power Laser Science and Engineering **11**, e93 (2023) doi:10.1017/hpl.2023.83.

https://doi.org/10.1017/hpl.2025.10073 Published online by Cambridge University Press

35. E. Kocharovskaya, M. Martyanov, and E. Khazanov, "Fluence noise dynamics of a laser pulse passing through an optical system with spatio-temporal dispersion", JOSA B accepted (2025)
36. H. Huang and T. Kessler, "Tiled-grating compressor with uncompensated dispersion for near-field-intensity smoothing", Optics Letters **32**, 1854-1856 (2007) •https://doi.org/10.1364/OL.32.001854.
37. X. Shen, S. Du, W. Liang, P. Wang, J. Liu, and R. Li, "Two-step pulse compressor based on asymmetric four-grating compressor for femtosecond petawatt lasers", Applied Physics B **128**, 159 (2022) https://doi.org/10.1007/s00340-022-07878-9.
38. E. Khazanov, "2D-smoothing of laser beam fluctuations in optical compressor", Laser Phys. Lett. **20**, 125001 (2023) https://doi.org/10.1088/1612-202X/ad00ab.
39. S. Du, X. Shen, W. Liang, P. Wang, J. Liu, and R. Li, "A 100-PW compressor based on single-pass single-grating pair", High Power Laser Science and Engineering **11**, e4 (2023) 10.1017/hpl.2023.5.
40. W. Liang, S. Du, R. Chen, X. Wang, X. Liu, X. Chen, X. Shen, J. Liu, and R. Li, "Viability verification of asymmetric four-grating compressor in SEL-100 PW frontend", Optics Communications **557**, 130317 (2024) https://doi.org/10.1016/j.optcom.2024.130317.
41. D. E. Kiselev, A. A. Kochetkov, I. V. Yakovlev, and E. A. Khazanov, "Experimental study of laser beam fluence fluctuation smoothing in asymmetric compressors", Applied Optics **63**, 9146-9151 (2024) https://doi.org/10.1364/AO.542361.
42. W. Liang, S. Du, R. Chen, X. Wang, X. Liu, X. Chen, X. Shena, J. Liu, and R. Li, "Viability verification of asymmetric four-grating compressor in SEL-100 PW frontend", Optics Communications **55**, 130317 (2024) https://doi.org/10.1016/j.optcom.2024.130317.
43. E. Khazanov, A. Shaykin, I. Kostyukov, V. Ginzburg, I. Mukhin, I. Yakovlev, A. Soloviev, I. Kuznetsov, S. Mironov, A. Korzhimanov, D. Bulanov, I. Shaikin, A. Kochetkov, A. Kuzmin, M. Martyanov, V. Lozhkarev, M. Starodubtsev, A. Litvak, and A. Sergeev, "Exawatt Center for Extreme Light Studies (XCELS)", High Power Laser Science and Engineering **11**, e78 (2023) 10.1017/hpl.2023.69.
44. M. Martyanov and E. Khazanov, "Pulse fluence noise dynamics at free space propagation", JOSA A, 1507-1514 (2023) https://doi.org/10.1364/JOSAA.496223.
45. E. A. Khazanov, A. A. Kochetkov, and D. E. Silin, "Spectrum of spatial noise of laser beam after reflection from nonideal surface", Radiophysics and Quantum Electronics **66**, 469-478 (2023) 10.1007/s11141-024-10308-9.
46. X. Wang, X. Liu, X. Lu, J. Chen, Y. Long, W. Li, H. Chen, X. Chen, P. Bai, Y. Li, Y. Peng, Y. Liu, F. Wu, C. Wang, Z. Li, Y. Xu, X. Liang, Y. Leng, and R. Li, "13.4 fs, 0.1 Hz OPCPA Front End for the 100 PW-Class Laser Facility", Ultrafast Science **2022**, 9894358 (2022) https://doi.org/10.34133/2022/9894358.
47. N. Khodakovskiy, M. Kalashnikov, E. Gontier, F. Falcoz, and P.-M. Paul, "Degradation of picosecond temporal contrast of Ti:sapphire lasers with coherent pedestals", Optics Letters **41**, 4441-4444 (2016) •https://doi.org/10.1364/OL.41.004441.
48. "Product cleanliness level and comtamination control program MIL-STD-1246C", (1987)
49. I. F. Stowers, J. A. Horvath, J. A. Menapace, A. K. Burnham, and S. A. Letts, "Achieving and maintaining cleanliness in NIF amplifiers", Proc. of SPIE **3492**, 609-620 (1998)
50. E. Khazanov, "Dependence of the focal intensity of a femtosecond laser pulse on the non-flatness of compressor diffraction gratings", High Power Laser Science and Engineering **12**, e85 (2024) doi:10.1017/hpl.2024.58.

51. E. L. Church, "Fractal surface finish", Applied Optics **27**, 1518-1526 (1988) https://doi.org/10.1364/AO.27.001518.
52. S. Liu, C. Jin, Y. Zhou, Y. Bai, Y. Zhao, K. Yi, and J. Shao, "Investigation on measurement of mid-frequency wavefront error for large optics in high-power laser system," in *Optical Measurement Systems for Industrial Inspection IX*, 2015), 952536-952531–952536-952511, 10.1117/12.2184586.
53. A. Duparre´, J. Ferre-Borrull, S. Gliech, G. Notni, J. Steinert, and J. M. Bennett, "Surface characterization techniques for determining the root-mean-square roughness and power spectral densities of optical components", Applied Optics **41**, 154-171 (2022) •https://doi.org/10.1364/AO.41.000154.
54. C. Hu, S. Wan, G. Jiang, H. Gu, Y. Zhang, Y. Jin, S. Liu, C. Zhao, H. Cao, C. Wei, and J. Shao, "Specifications and control of spatial frequency errors of components in two-beam laser static holographic exposure for pulse compression grating fabrication", High Power Laser Science and Engineering **12**, e1 (2024) 10.1017/hpl.2023.81.
55. A. L. Camus, H. Coic, N. Blanchot, S. Bouillet, E. Lavastre, M. Mangeant, C. Rouyer, and J. Néauport, "Impact of compression grating phase modulations on beam over-intensities and downstream optics on PETAL facility", Optics Express **30**, 7426-7440 (2022) •https://doi.org/10.1364/OE.449397.
56. J. E. Harvey, S. Schröder, N. Choi, and A. Duparré, "Total integrated scatter from surfaces with arbitrary roughness, correlation widths, and incident angles", Optical Engineering **51**, 013402 (2012) https://doi.org/10.1117/1.OE.51.1.013402.
57. R. D. Boyd, J. A. Britten, D. E. Decker, B. W. Shore, B. C. Stuart, M. D. Perry, and L. Li, "High-efficiency metallic diffraction gratings for laser applications", Applied Optics **34**, 1697-1706 (1995) 10.1364/AO.34.001697.
58. S. Mironov, V. Lozhkarev, G. Luchinin, A. Shaykin, and E. Khazanov, "Suppression of small-scale self-focusing of high-intensity femtosecond radiation", Applied Physics B **113**, 147-151 (2013) 10.1007/s00340-013-5450-1.
59. E. A. Khazanov, S. Y. Mironov, and G. Mourou, "Nonlinear compression of high-power laser pulses: compression after compressor approach", Physics-Uspekhi **62**, 1096-1124 (2019) https://doi.org/10.3367/UFNe.2019.05.038564.

https://doi.org/10.1017/hpl.2025.10073 Published online by Cambridge University Press